https://doi.org/10.5194/egusphere-2026-4400
Preprint. Discussion started: 5 August 2026

Millennial-scale sensitivity of Pine Island and Thwaites Glaciers to effective pressure and ocean melt parameterisations

Matt Trevers[1], Stephen L. Cornford[1], and Antony J. Payne[2]

[1]Centre for Polar Observation and Modelling, School of Geographical Sciences, University of Bristol, Bristol, UK
[2]School of Environmental Sciences, University of Liverpool, Liverpool, UK

Correspondence: Matt Trevers (matt.trevers@bristol.ac.uk)

Abstract. Pine Island and Thwaites Glaciers, situated in the Amundsen Sea Embayment in West Antarctica, are the two largest modern-day contributors of sea level rise from Antarctica, and their potential future retreat threatens the stability of the West Antarctic Ice Sheet over coming centuries. Here we present numerical simulations exploring the sensitivity of both glaciers to reducing the basal friction (bed-weakening) in response to ice thinning and the rate of ice shelf melting over millennial timescales. We find that bed-weakening leads to faster rates of retreat and sea level rise when confined to the grounding zone, but expanding the region of bed-weakening delayed retreat instead. Pine Island Glacier is highly sensitive to increases in the ocean melt rate, while Thwaites Glacier is more sensitive to bed-weakening. The sea level contribution from Thwaites Glacier over the next century is particularly insensitive to changes in ocean melting. Despite the relatively weak buttressing from the Thwaites Ice Shelf, it still provides sufficient support locally to suppress the rapid retreat that occurred with the complete removal of all floating ice. These results highlight the sensitivity of sea level projections to the relatively poorly known basal effective pressure, and the need for future ice flow models to be coupled with with highly-skilled basal hydrology models.

1 Introduction

The neighbouring Pine Island and Thwaites Glaciers, located in the Amundsen Sea Embayment (ASE) of West Antarctica (Figure 1), have been the two largest contributors to sea level rise (SLR) from the Antarctic Ice Sheet in recent decades. In 2017 the rates of sea level contribution were 0.16 mm yr^{-1} and 0.1 mm yr^{-1} from Pine Island Glacier (PIG) and Thwaites Glacier (TG) respectively (Rignot et al., 2019). These losses are ocean-forced, with enhanced transport of Circumpolar Deep Water towards their grounding lines (Jenkins et al., 2016; Holland et al., 2019) driving rapid melting of their floating ice shelves (Dutrieux et al., 2013; Naughten et al., 2022). This causes a loss of buttressing, driving acceleration and thinning of upstream grounded ice and grounding line retreat. Both glaciers rest on beds that slope downward towards the ice sheet interior, a configuration which can give rise to accelerating retreat through marine ice sheet instability (MISI; Weertman, 1974; Schoof, 2007).

PIG and TG have been the subject of many modelling studies (e.g. Joughin et al., 2010b, 2014; Favier et al., 2014; Nias et al., 2016; Seroussi et al., 2017; Alevropoulos-Borrill et al., 2020; Barnes and Gudmundsson, 2022), which indicate a divergence in their response to melting of their ice shelves. Gudmundsson et al. (2023) showed that the Pine Island Ice Shelf

https://doi.org/10.5194/egusphere-2026-4400
Preprint. Discussion started: 5 August 2026

(PIIS) provides substantial buttressing to the flow of upstream ice, while the buttressing provided by the Thwaites Ice Shelf (TIS) is much more limited and localised to small-scale features of the grounding line profile. The PIIS is confined within an embayment and occasionally calves large tabular icebergs from its front. By contrast, the TIS has degraded significantly in recent decades and is no longer a single solid body of ice (Miles et al., 2020). Instead, it has effectively separated into the more continuous Thwaites Eastern Ice Shelf which remains pinned on a seafloor ridge near its calving front, and the Thwaites Western Ice Tongue, which is a highly fragmented mélange of large icebergs and sea ice (Miles et al., 2020; Benn et al., 2022). Although it appears likely that the collapse of the TIS may occur in the coming decades (Wild et al., 2022), this is not expected to have a major impact on the flow of the grounded glacier (Gudmundsson et al., 2023).

Basal friction is a key control on the flow dynamics of ice streams, and the form of a basal sliding law remains a significant uncertainty in ice sheet model projections. "Weertman" sliding rules (i.e. a power-law relationship between sliding speed and basal shear stress with an index of $\sim \frac{1}{3}$, Weertman, 1957) are frequently employed to describe sliding over hard beds (e.g. Brondex et al., 2017; Nias et al., 2018; Barnes and Gudmundsson, 2022). However this fails to account for the effect of cavitation at the bed or of bed deformation. Recent studies have shown that Coulomb-like behaviour provides a good approximation for both sliding over a deformable till and fast sliding with cavitation over a hard bedrock (Gagliardini et al., 2007; Zoet and Iverson, 2020; Minchew and Joughin, 2020), leading to the formulation of sliding laws that incorporate both Weertman and Coulomb regimes (Joughin et al., 2019).

Inverse methods are typically used to infer the values of friction coefficients in sliding laws (MacAyeal, 1993), although single snapshot inversions are unable to determine the form of the sliding law or isolate the dependence on basal effective pressure ($N = P_i - P_w$, where P_i and P_w are the ice overburden and water pressure respectively), which is generally subsumed into the coefficient values. Other sliding laws explicitly separate out basal effective pressure (e.g. Schoof, 2005; Tsai et al., 2015), although this is difficult to constrain without detailed knowledge of subglacial hydrology. Joughin et al. (2010b) introduced a bed-weakening scheme in which the basal friction is reduced as ice thins towards flotation below a critical height above flotation to account for the reduction in effective pressure and accurately model the sensitivity to ocean melting.

In this study, we examine the sensitivity of PIG and TG to the ice shelf melt parameterisation and bed-weakening over millennial timescales, by varying the critical height above flotation and the coefficient controlling the ice shelf basal melt rate. Although our study may appear superficially similar to Joughin et al. (2024), there are clear differences in our goals and experimental design: we apply melting separately to PIG and TG to examine their individual responses, and our simulations run for much longer timescales. We also apply a parameterised ice shelf melt rate rather than a prescribed melt volume to simulate how melt rates might change in response to changes in ice shelf geometry. Additionally we probe a larger range of the critical height above flotation to apply bed-weakening across a wider region.

https://doi.org/10.5194/egusphere-2026-4400
Preprint. Discussion started: 5 August 2026

2 Methods

2.1 BISICLES ice sheet model

In this study, we use the BISICLES ice sheet model (Cornford et al., 2013), which has been used in previous studies of the Antarctic Ice Sheet (e.g. Cornford et al., 2015; Nias et al., 2016; Martin et al., 2019; Alevropoulos-Borrill et al., 2020; O'Neill et al., 2025). BISICLES is a vertically-integrated ice flow model based on the L1L2 approximation (Schoof and Hindmarsh, 2010), which uses adaptive mesh refinement (AMR) to refine the grid around the grounding line and in fast flowing ice streams.

The computational domain which covers the full basins of the PIG and TG, as well as the Pope, Smith and Kohler Glaciers and the Crosson and Dotson Ice Shelves, is shown in Figure 1. We use a 4 km grid inland with three levels of AMR to produce a finest grid resolution of 500 m around the grounding line. A present-day ASE state, produced through an iterative inversion-relaxation procedure, comprises fields of basal friction coefficient C, ice stiffening factor ϕ and ice thickness which are consistent with observed ice velocity and thinning rates. This procedure, which follows Bevan et al. (2023) and van den Akker et al. (2025), is described in Supplementary Text S1. The basal shear stress calculated by the initial inversion is shown in Figure 2a in the vicinity of the PIG and TG grounding lines. The bed topography and pre-initialisation ice thickness were provided by BedMachine v3 (Morlighem et al., 2020; Morlighem, 2022). The surface accumulation rate, which was kept constant throughout simulations, came from the MAR regional climate model 1980 to 2018 mean (Agosta et al., 2019). A three-dimensional temperature field was generated by a thermal spin-up, described in Supplementary Text S2. Input fields for the model are shown in Supplementary Figure S3.

2.2 Basal sliding

The basal stress for grounded ice was determined by a Regularised Coulomb friction law equivalent to that introduced by Joughin et al. (2019),

$$\boldsymbol{\tau}_{\mathrm{b}} = -\lambda \cdot C\,|\boldsymbol{u}_{\mathrm{b}}|^{m-1}\left(\frac{|\boldsymbol{u}_{\mathrm{b}}|}{u_0}+1\right)^{-m}\cdot \boldsymbol{u}_{\mathrm{b}}, \tag{1}$$

where C is the spatially varying friction coefficient, $\boldsymbol{u}_{\mathrm{b}}$ the basal sliding velocity, $m = 1/3$ the friction law exponent, and $u_0 = 50$ m yr^{-1} the fast sliding speed. λ is a prefactor that weakens the bed as the glacier thins toward flotation by reducing the basal stress smoothly below some critical height above flotation (Joughin et al., 2010a),

$$\lambda = \begin{cases} \frac{(h-h_{\mathrm{f}})}{\min[h_0-h_{\mathrm{f}},h_{\mathrm{T}}]} & (h-h_{\mathrm{f}}) \le h_{\mathrm{T}} \\ 1 & \text{otherwise,} \end{cases} \tag{2}$$

where h is the ice thickness, h_{f} the flotation thickness, h_0 the initial ice thickness and h_{T} the critical height above flotation. Joughin et al. (2010a) found $h_{\mathrm{T}} = 41$ m to be appropriate for PIG using a regularised Coulomb friction law with $u_0 = 300$ m yr^{-1}. The inclusion of h_0 in Equation 2 ensures that $\lambda = 1$ everywhere at the beginning of the simulations, so that the basal

https://doi.org/10.5194/egusphere-2026-4400
Preprint. Discussion started: 5 August 2026

stress stress is consistent with the initialised model state. We limit $\lambda \leq 1$ to prohibit bed strengthening resulting from thickening in regions where $h_0 < h_\mathrm{T}$.

2.3 Basal melt parameterisation

We apply a simple depth-dependent basal melt rate parameterisation to floating ice. The melt rate for floating cells is calculated as

$$\dot{m} = a_\mathrm{m} \cdot a_0 \cdot \max\left[\left(d - d_\mathrm{tc}\right), 0\right]^p, \tag{3}$$

where d is the ice shelf draft, d_tc is the thermocline depth (above which no melting occurs), p is the melt rate index and the coefficient a_m is a melt rate multiplier. The coefficient a_0 is calculated such that for given values of p and d_tc, and with $a_\mathrm{m} = 1$, the melt rate integrated across the ice shelf area in its initial geometric configuration totals the observed melt rate $\sim$ 100 Gt yr^{-1} (Rignot et al., 2013). $a_\mathrm{m} = 1$ is therefore assumed to represent present day melt rates. The parameter values remain fixed during the course of a simulation, so the melt volume depends on the evolving ice shelf geometry.

The parameter values a_0 and p are determined separately for both the PIIS and TIS following a procedure described in Supplementary Text S3.

2.4 Experiments

We performed a series of simulations exploring ranges of the critical height above flotation h_T and the melt amplifier a_m. Simulations were carried out with melting applied individually to either the PIG or TG basins. TG melt experiments were carried out for 1000 years, while PIG melt experiments were carried out for 1500 years to account for the generally slower response of PIG.

For both PIG and TG, we ran two sets of simulations, which are detailed in Table 1. In simulation sets PIG1 and TG1, keeping $a_\mathrm{m} = 1$, we applied a range of values of h_T between 0 m and 500 m. The results of PIG1 and TG1 are shown in Section 3.1. In simulation sets PIG2 and TG2, for each of $h_\mathrm{T} = 0$ m, 41 m and 150 m, we applied a range of melt amplifier a_m values between 0.1 and 10. Complementary extreme melt simulations, in which floating ice was immediately removed to prohibit ice shelves, were also performed as part of PIG2 and TG2 for each h_T value. These results are shown in Section 3.2.1 for PIG2 and Section 3.2.2 for TG2.

3 Results

Figure 2 shows the distribution of basal shear stress near the grounding lines of PIG and TG, and how basal shear stress varies with height above flotation. Figure 2b shows a weakening of the bed for $h_\mathrm{T} \lesssim 200$ m for both glaciers. The weakening is stronger and more abrupt for TG, which has generally higher basal shear stresses. Limiting the analysis to regions of fast-flowing ice ($\geq$ 100 m yr^{-1}, Figure 2c) results in a similar picture for PIG, where basal shear stresses beneath fast-flowing ice

https://doi.org/10.5194/egusphere-2026-4400
Preprint. Discussion started: 5 August 2026

Simulation set	Drainage basin	h_{T} (m)	a_{m}	p	a_0
PIG1	Pine Island	0 to 500	1	2	9.07×10^{-5}
TG1	Thwaites	0 to 500	1	1	9.17×10^{-2}
PIG2	Pine Island	{0, 41, 150}	0.1 to 10, $\sim\infty$ (no shelves)	2	9.07×10^{-5}
TG2	Thwaites	{0, 41, 150}	0.1 to 10, $\sim\infty$ (no shelves)	1	9.17×10^{-2}

Table 1. Parameter values and ranges for the sets of simulations.

are elevated above the bed strength of surrounding slow-flowing regions. Although the bed weakening effect is less clear for PIG due to the small number of cells in the region of low h_{T} and fast flow, this analysis supports the use of a mechanism to weaken the bed beneath ice near flotation, and suggests that $h_{\mathrm{T}} \sim 200$ m may be the most appropriate threshold for initiating bed weakening.

3.1 Critical height above flotation

Figure 3 shows how the response of PIG to melting of PIIS varies across a range of values of h_{T} in the PIG1 simulations. The results show the close association between mass loss (Figure 3a) and grounding line retreat (Figure 3b). Grounding lines retreated in a series of stages with intermittent periods of stagnation, reflecting the topography of the underlying bedrock. The $h_{\mathrm{T}} = 0$ m simulation stabilised after just 25 km of grounding line retreat, resulting in less than 5 cm of SLC. In simulations with larger h_{T}, rapid grounding line retreat of up to 4 km yr^{-1} (Supplementary Figure S6) across a bedrock overdeepening occurred once the grounding line had crossed a threshold ∼100 km upstream of its initial position. This phase of rapid retreat coincides with a pronounced increase in the rate of mass loss up to 1.5 mm yr^{-1} SLE (sea level equivalent).

In general there is strong sensitivity to h_{T} for small values of h_{T}, with decreasing sensitivity as h_{T} increases. At 200 and 500 years the response to further increases in h_{T} saturates above ∼150 m (Supplementary Figure S7). Rapid grounding line retreat was triggered sooner with increasing h_{T} up to $h_{\mathrm{T}} \sim 250$ m; for higher h_{T} rapid grounding line retreat was actually triggered later, although at increasingly rapid rates once it has been triggered. This produced maximums in the plots in Supplementary Figure S7, whereby increasing h_{T} above ∼250 m produced less total SLC at 1000 and 1500 years (yellow and red lines). After 1500 years the SLC had saturated at ∼45 cm in a number of simulations, indicating almost complete deglaciation of the PIG drainage basin.

Maps of grounding lines in Figure 4 show that retreat in the $h_{\mathrm{T}} = 500$ m simulation was delayed relative to simulations with lower h_{T}. This reversal of sensitivity with increasing h_{T} is explained by higher values of h_{T} causing bed weakening further inland for the same amount of thinning, driving accelerated ice flow over a wider region. Although this produces thinning across a larger area, it also results in an initially enhanced transport of ice to the grounding line, limiting the rate of thinning

https://doi.org/10.5194/egusphere-2026-4400
Preprint. Discussion started: 5 August 2026

there. By contrast, lower values of h_T concentrate acceleration and thinning closer to the grounding line, producing a steeper surface slope and hence faster thinning of the grounding line, leading to earlier retreat. This effect is demonstrated by Supplementary Movie S1 which compares thickness changes for PIG for $h_\mathrm{T} = 200$ m and 500 m.

Figure 5 shows the results from the equivalent TG1 simulations for the TG basin, with corresponding maps of the grounding lines at selected points during the simulations in Figure 6. As for PIG, grounding line retreat for TG was interrupted by intermittent periods of temporary stabilisation on a series of ridges upstream of the present-day grounding line (e.g Yu et al., 2018). Beyond ∼150 km there are no further topographical obstacles, and the grounding line retreats very rapidly for a further 150 km. This retreat is even more rapid than for PIG, with grounding line retreat rates of up to 8 km yr^{-1} and mass loss rates of nearly 3 mm yr^{-1} SLE (Supplementary Figure S8). In general, increasing h_T drives rapid retreat and mass loss earlier in the simulation (Supplementary Figure S9). As for PIG, there is a maximum at $h_\mathrm{T} \sim 300$ m, beyond which further increases in h_T delayed the onset of rapid grounding line retreat and mass loss. The cause of this delay is the same mechanism as we inferred for PIG: increased thinning across a wider region with higher h_T increases the flow of ice to the grounding line, delaying grounding line retreat relative to smaller h_T values.

Supplementary Movies S2 and S3 correspond to Figures 4 and 6.

3.2 Ice shelf melting

3.2.1 Pine Island Glacier

Figure 7 shows the results of the PIG2 simulations for PIG with varying melt rates. The melt amplifier a_m was varied between 0.1 and 10 for h_T values of 0 m, 41 m and 150 m. As expected, increasing values of both h_T and a_m cause rapid retreat and mass loss to occur earlier in the simulation and more rapidly. For $h_\mathrm{T} = 0$ m and $a_\mathrm{m} < 1$ retreat stagnates early and the total sea level contribution does not exceed 5 cm. For $a_\mathrm{m} < 1$, bed-weakening (i.e. $h_\mathrm{T} > 0$) is required to initiate more substantial retreat. The sensitivity to h_T appears to be greatest for $a_\mathrm{m} \sim 1$, and decreases with increasing a_m.

Supplementary Figure S10 shows that most of the sensitivity to changes in the melt rate occurs for $a_\mathrm{m} > 1$, indicated by the steep gradients in SLC on the right hand side of the vertical black line. Sea level contribution saturates at ∼ 45 cm SLE after 1500 years for $a_\mathrm{m} > 1$, indicating full deglaciation of the PIG basin. This saturation was reached earlier for higher values of h_T and a_m. For $h_\mathrm{T} = 150$ m and $a_\mathrm{m} > 5$ full deglaciation was achieved by 500 years.

Complementary simulations were carried out in which ice shelves were completely removed to represent the upper limit of extreme melting (red lines in Figure 7). These result in extremely rapid grounding line retreat exceeding 300 km in less than 100 years for all three h_T values, and with corresponding very high rates of mass loss. This clearly demonstrates that the stability of PIG is strongly dependent on the buttressing from PIIS.

https://doi.org/10.5194/egusphere-2026-4400
Preprint. Discussion started: 5 August 2026

Supplementary Figures S11 to S13 show grounding line maps for PIG melt simulations for $h_{\mathrm{T}} = 0$ m, 41 m and 150 m respectively. Supplementary movies S4 to S6 correspond to Supplementary Figures S11 to S13.

3.2.2 Thwaites Glacier

TG is far less sensitive to increasing melt than PIG in the equivalent TG2 simulations, so that h_{T} is the major control (Figure 8). This is immediately clear from Figure 8a in which the SLC is grouped by h_{T}. All $h_{\mathrm{T}} = 0$ m simulations saw very little retreat or mass loss, with no more than 3 cm SLE, and exhibited no sensitivity to a_{m}. The sensitivity to increasing a_{m} for $h_{\mathrm{T}} > 0$ is less significant than for PIG; increasing a_{m} from 1 to 8 only roughly doubled the rate of mass loss for both $h_{\mathrm{T}} = 41$ m and $h_{\mathrm{T}} = 150$ m. This is highlighted in Supplementary Figure S14, in which the time taken to reach a certain SLC for $a_{\mathrm{m}} = 1$ is consistently approximately double the time taken for the same SLC for $a_{\mathrm{m}} = 8$, for both $h_{\mathrm{T}} = 41$ m and $h_{\mathrm{T}} = 150$ m. For PIG the equivalent delay for $a_{\mathrm{m}} = 1$ delay is a larger ratio and varies significantly throughout the retreat and between h_{T} values.

The extreme melt simulations (red lines in Figure 8) produced slower rates of retreat for TG compared with the equivalent experiments for PIG, although still at significantly higher rates than the corresponding $a_{\mathrm{m}} = 8$ simulations. Notably the $h_{\mathrm{T}} = 0$ m extreme melt simulation resulted in full deglaciation after several hundred years. By contrast, the presence of floating ice in all other $h_{\mathrm{T}} = 0$ m simulations resulted in very limited retreat and mass loss. In the $a_{\mathrm{m}} = 10$ case, the grounding line retreated approximately 20 km and a narrow ice shelf formed.

Unlike for PIG, most of the sensitivity to increasing melt rates occurs for $a_{\mathrm{m}} < 1$ (Supplementary Figure S15 , c.f. Supplementary Figure S10 for PIG). At 1000 years (orange lines) SLC has already saturated at its maximum of nearly 60 cm SLE at $a_{\mathrm{m}} \geq 1$ for $h_{\mathrm{T}} = 150$ m, and at $a_{\mathrm{m}} \geq 2$ for $h_{\mathrm{T}} = 41$ m. At earlier time snapshots, increasing a_{m} above 1 does not lead to big increases in the SLC. This suggests that future increases in the melt rate will only have a relatively small impact on the rate and timing of retreat. On the other hand, Supplementary Figure S15 shows enhanced sensitivity to h_{T}, shown by the larger offsets between lines of the same colour relative to the equivalent plots in Supplementary Figure S10.

Finally, the SLC after 100 years shows low sensitivity to the melt rate (blue lines in Supplementary Figure S15, reproduced in greater detail in Supplementary Figure S16). Even for $h_{\mathrm{T}} = 150$ m, varying a_{m} from 0.1 to 10 only produced a four-fold increase in total mass loss.

Supplementary Figures S17 and S18 show grounding line maps for TG melt simulations for $h_{\mathrm{T}} = 41$ m and 150 m respectively. Supplementary movies S7 and S8 correspond to Supplementary Figures S17 and S18 respectively.

https://doi.org/10.5194/egusphere-2026-4400
Preprint. Discussion started: 5 August 2026

4 Discussion

Our simulations showed that PIG is highly sensitive to the rate of ice shelf melting, while TG is more sensitive to stress conditions at its bed. We attribute the differing behaviour to PIG being largely supported by buttressing from PIIS. On the other hand TG is largely supported by the ridge of elevated bedrock which extends upstream of the grounding line. Very rapid retreat only occurs once the grounding line has retreated beyond this ridge (Yu et al., 2018). These results are in line with the findings of other recent modelling studies focused on the ASE. Barnes and Gudmundsson (2022) found that TG was significantly less sensitive to changes in the melting or even collapse of its ice shelf than PIG. Gudmundsson et al. (2023) showed that the TIS provides only minimal buttressing to upstream ice, in contrast with the PIIS which produced much more significant buttressing. The initial removal of the TIS in their simulations produced only a few mm additional SLC over a century, while removing the PIIS produced an order of magnitude greater effect. Benn et al. (2022) also found that further weakening or unpinning of the TIS had little impact on future losses from TG.

Our experiments produced contrasting short-term responses for PIG and TG. Supplementary Figure S16 shows that the centennial SLC from TG is very insensitive to increasing melt. Without progressive bed weakening, there is essentially no difference in outcomes across the range of melt rate. Even with substantial bed weakening, a tenfold increase in the melt parameter produced only a doubling of SLC. For PIG the opposite is true, with bed weakening playing the minor role compared to increasing the melt parameter. This implies that the evolution of TG over the 21st Century is largely already pre-determined, and unlikely to be affected by changes in ocean temperatures, whereas PIG's behaviour over the same period is strongly dependent on ocean conditions. Our results also suggest that it will be difficult to make inferences about the longer term behaviour of TG based on observations over the 21st Century, since there is divergence in the mass loss rates with changes in both the melt parameter and the strength of bed weakening over several centuries.

This near-future insensitivity of TG to the melt parameter might at first glance appear to contradict Joughin et al. (2024), who found that the SLC scaled linearly with the total melt volume for both glaciers. We note that the total melt volume is not necessarily proportional to the melt parameter since it depends upon the evolving ice shelf geometry. Supplementary Figures S19 and S20 show time-series of SLC and cumulative melt volume over 200 years for both glaciers, and the ratios of SLC to melt for the same period respectively. They show that the sensitivity to ice shelf melting is similar for PIG and TG, broadly in line with Joughin et al. (2024), although TG sees less overall melt and SLC. The sensitivity to ice shelf melting for TG was also more strongly dependent on the strength of bed-weakening. This is likely because the lack of buttressing provided by the TIS means that increased melting does not significantly increase the grounding line discharge, meaning that the supply of ice available for melting is not replenished at the same rate as for PIG.

One notable result was the rapid retreat of TG in the absence of bed-weakening when floating ice was prohibited (dotted red lines, Figure 8), which was in stark contrast to the limited retreat when ice shelves were allowed to form. This shows

https://doi.org/10.5194/egusphere-2026-4400
Preprint. Discussion started: 5 August 2026

that while the overall buttressing from the TIS is weak, even the remnant ice shelf after several centuries of melting provides sufficient localised buttressing in concavities of the grounding line to prohibit retreat in those regions (Gudmundsson et al., 2023), which would otherwise lead to full deglaciation of the TG drainage basin after several hundred years in the absence of floating ice.

4.1 Towards coupled basal hydrology models

Our study demonstrates the importance of coupling models of basal hydrology into future ice sheet models (e.g. Kazmierczak et al., 2022; Lu and Kingslake, 2024). The bed-weakening prefactor λ represents the reduction in basal friction resulting from unknown high basal water pressure in the region near the grounding line. Some sliding rules explicitly include the basal effective pressure as a component of the basal friction (e.g. Lliboutry, 1968; Budd et al., 1979). An alternative approach proposed by Tsai et al. (2015) calculates the basal shear stress as the minimum of the Coulomb friction, which is a function of the effective pressure, and the Weertman friction. We might expect this rule to produce a similar distribution of basal shear stress to that seen in Figure 2, and therefore h_{T} may represent the threshold between Coulomb and Weertman regimes.

Supplementary Figure S21 shows that $h_{\mathrm{T}} = 200$ m corresponds to an inland distance of 3 to 4 km upstream of the grounding line. This length scale is comparable to (although slightly shorter than) the widths of proposed grounding zones and ocean water intrusion zones for TG in previous studies (Parizek et al., 2013; Rignot et al., 2024), suggesting that the value of h_{T} may be linked to the inland loss of ocean connectivity. Future ice sheet models could therefore be coupled with basal hydrology models by replacing λ with N/N_0, where N is the basal effective pressure produced by a hydrology model and N_0 is some reference pressure. This approach is beyond the scope of this study but warrants consideration in future work.

5 Conclusions

We have carried out millennial-scale simulations of the evolution of the PIG and TG in response to varying melt rate and bed weakening parameters. The results of our simulations are broadly consistent with previous studies, while also revealing some novel findings. Increasing the critical height above flotation for bed weakening initially produced higher rates of mass loss. However, increasing this threshold past a certain point resulted in delayed retreat rates, due to the increased ice flux to the grounding line and the relatively lower rate of surface steepening. We found that PIG was highly sensitive to melt rate increases through varying the melt multiplier, while TG was more sensitive to weakening of its bed. However, even under high-melt conditions, the remnant ice shelf still provided sufficient localised buttressing to TG to prevent the catastrophic retreat that resulted when ice shelves were completely prohibited. TG is very insensitive to increases in the melt amplifier over the next century for all values of the critical height above flotation, making it difficult to predict how its SLC will evolve in future centuries. Further analysis showed that the SLC of both PIG and TG is broadly proportional with the melt volume from their ice shelves.

Our simulations demonstrate the necessity for the application of a bed-weakening scheme in marine ice sheet models. We

https://doi.org/10.5194/egusphere-2026-4400
Preprint. Discussion started: 5 August 2026

suggest that for these glaciers, the optimal threshold for bed weakening may be a height above flotation of ∼200 m. The need for this parameterisation highlights the necessity for a better understanding of basal hydrology and its impact on ice stream dynamics, and for coupling of basal hydrology and ice flow models to provide more accurate projections of future sea level rise.

https://doi.org/10.5194/egusphere-2026-4400
Preprint. Discussion started: 5 August 2026

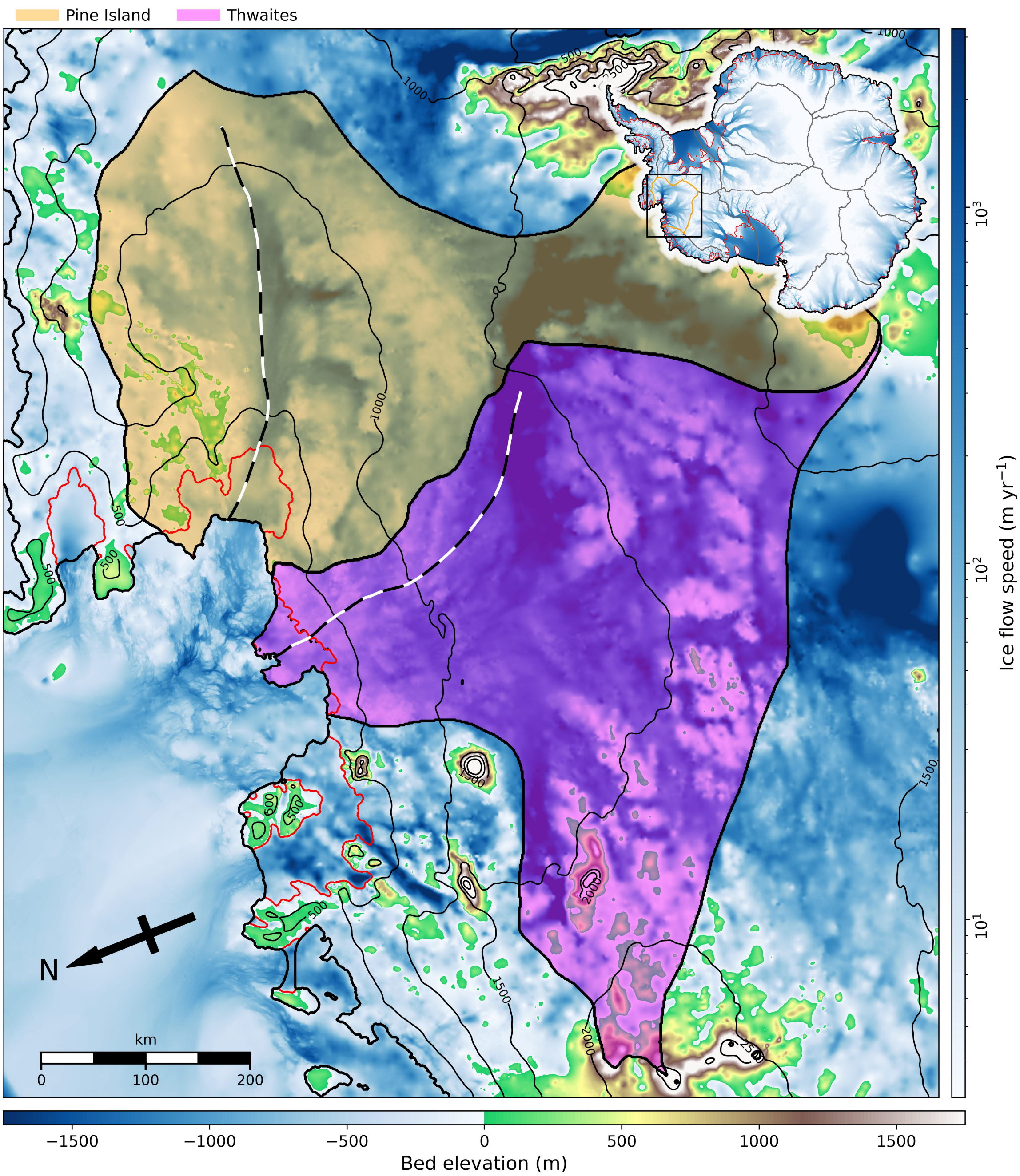

Figure 1. Bed topography of the ASE computational domain, with the PIG and TG basins highlighted. Thick black lines show the initial ice front extent and basin boundaries, red lines the initial grounding line, thin black contours ice surface elevation and dashed black and white lines flowlines used in this study. The inset map shows Antarctic-wide flow speeds (Mouginot et al., 2019) with basin boundaries from Zwally et al. (2012). The black box shows the extent of the ASE domain within Antarctica.

https://doi.org/10.5194/egusphere-2026-4400
Preprint. Discussion started: 5 August 2026

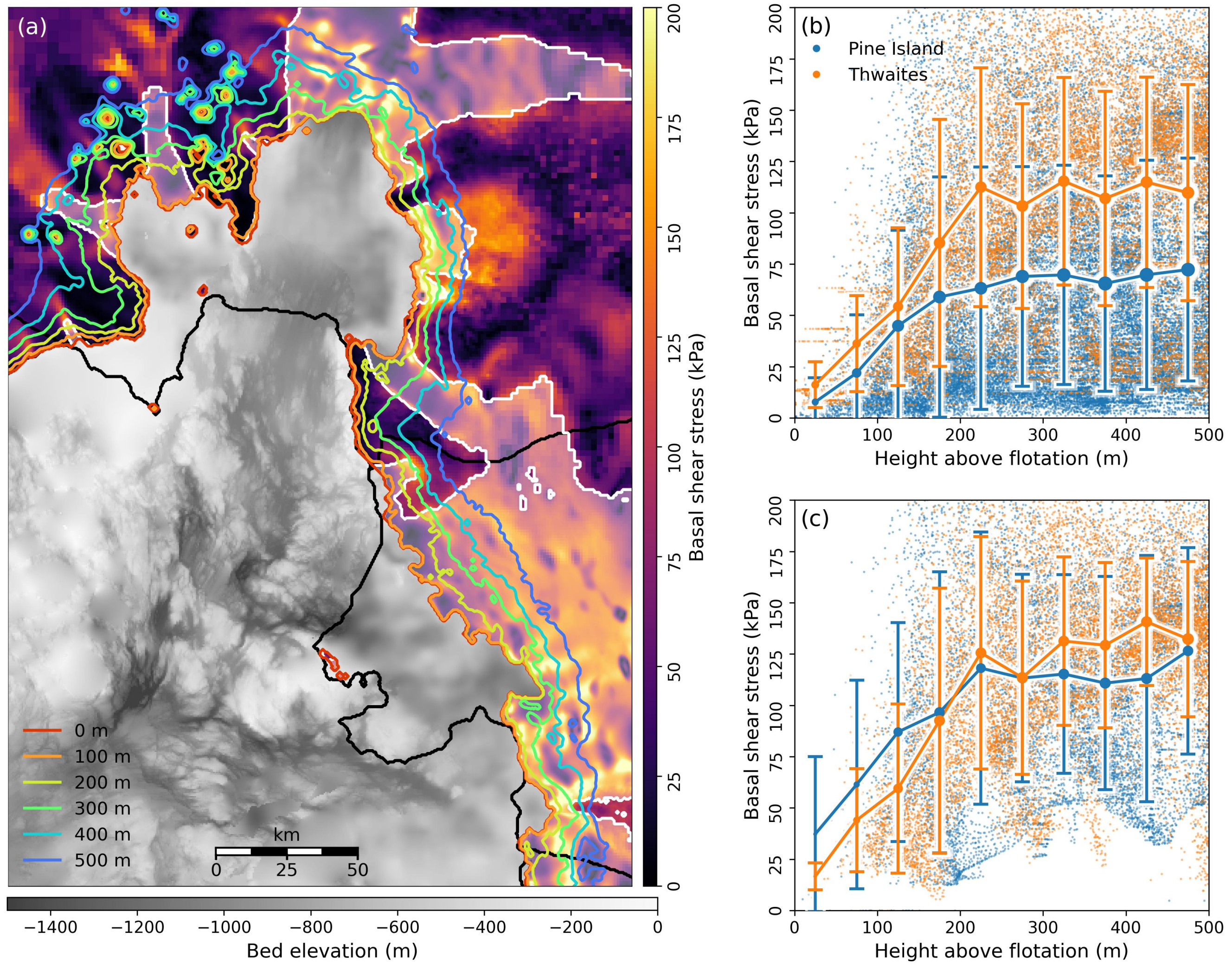

Figure 2. (a) Map of inverted basal shear stresses in the PIG and TG grounding zones. Coloured lines indicate contours of thickness above flotation $(h - h_\mathrm{f})$ up to 500 m. Red lines (0 m) indicate the grounding line. The white shaded area corresponds to ice flow speeds in excess of 100 m yr^{-1}. Basal stresses and thickness above flotation contours were calculated for the BedMachine v3 ice geometry prior to any relaxation during the model initialisation procedure. (b) Basal shear stresses plotted against the height above flotation in the PIG and TG basins. Small points denote individual cell values. Larger connected points are the mean basal shear stress calculated for 50 m bins of height above flotation. The error bars are calculated as the standard deviation on the mean, and the marker sizes indicate the relative number of cells within each bin. (c) Basal shear stresses plotted against the height above flotation as in (b), but for cells with ice flow speeds in excess of 100 m yr^{-1} (white shaded region in (a)).

https://doi.org/10.5194/egusphere-2026-4400
Preprint. Discussion started: 5 August 2026

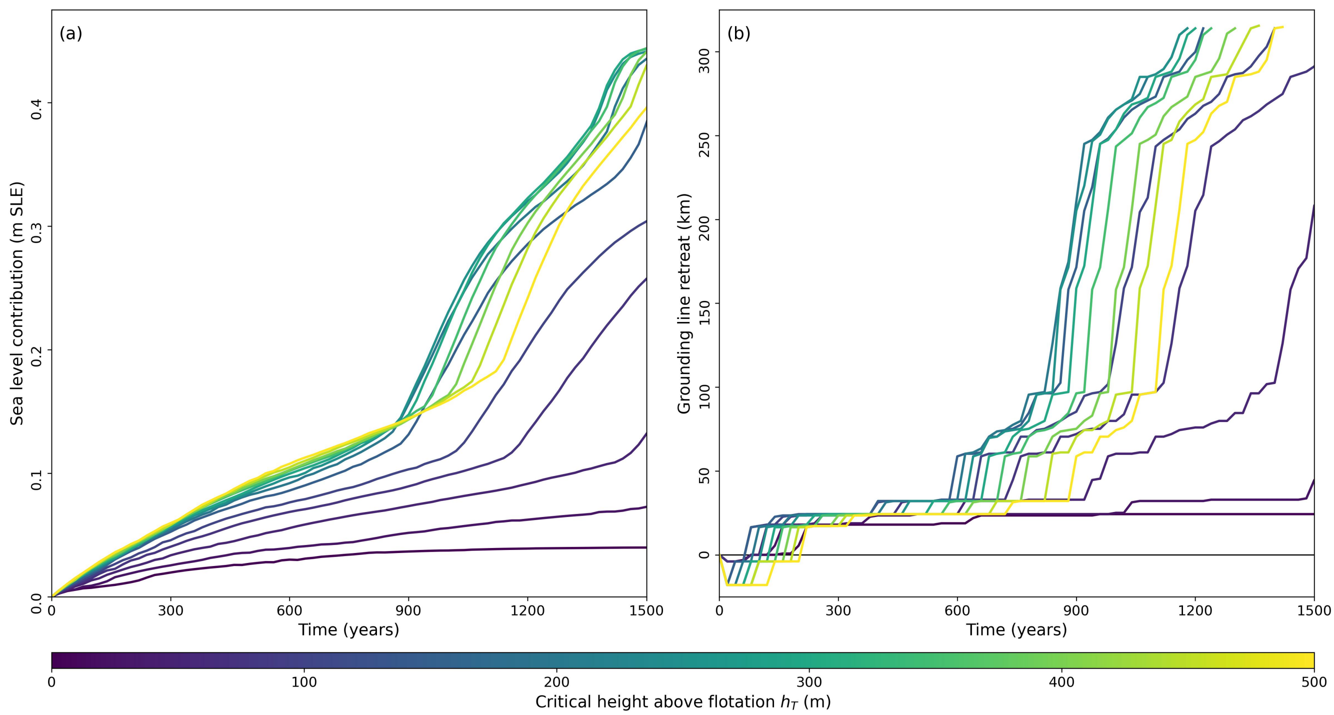

Figure 3. Results for PIG1 simulations across the range of h_T. (a) The change in SLC within the PIG basin. (b) The grounding line retreat measured along the PIG flowline.

https://doi.org/10.5194/egusphere-2026-4400
Preprint. Discussion started: 5 August 2026

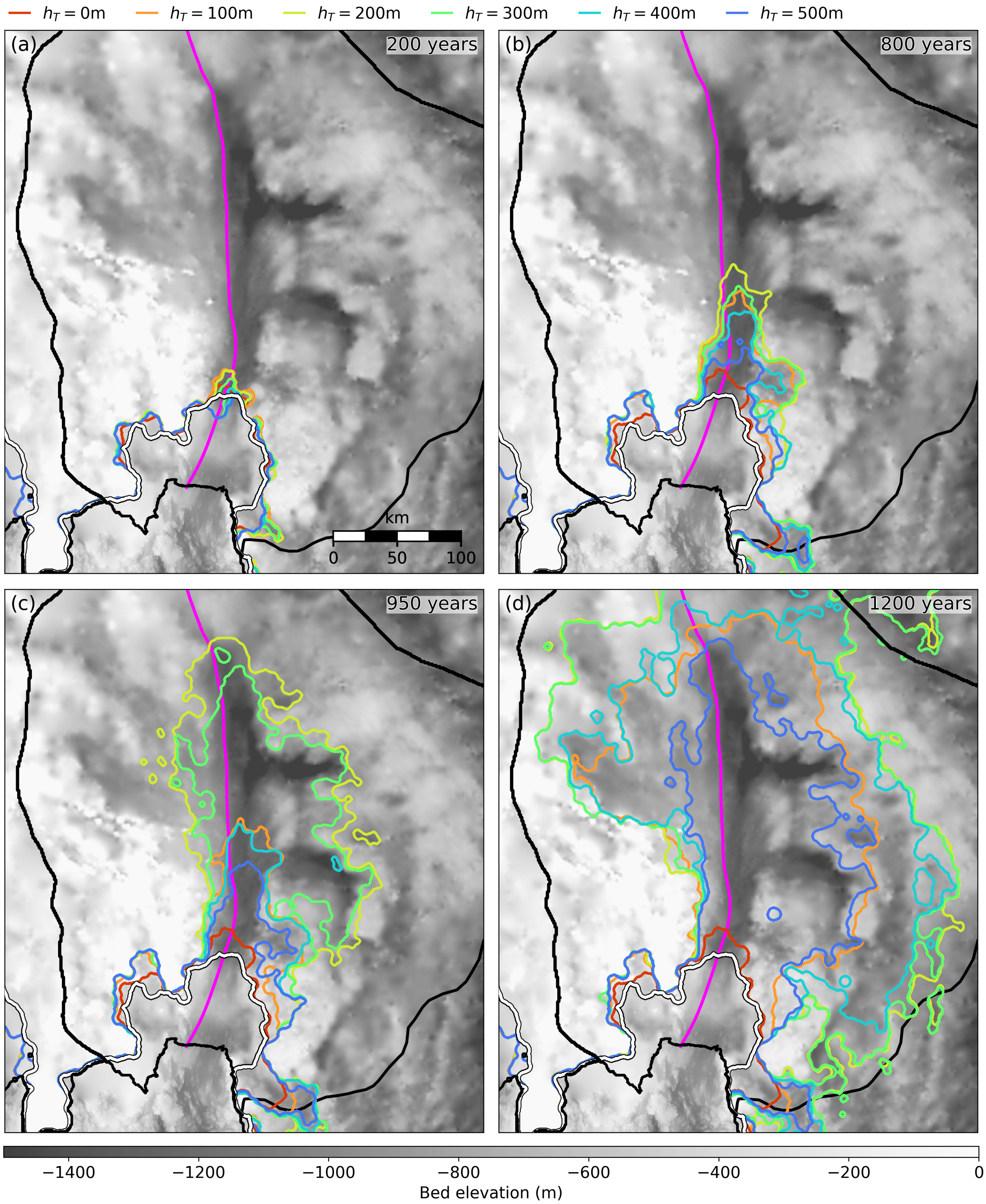

Figure 4. Maps of grounding line retreat for PIG1 simulations (Figure 3), across the range of h_T. Snapshots at 200 years (a), 800 years (b), 950 years (c) and 1200 years (d).

https://doi.org/10.5194/egusphere-2026-4400
Preprint. Discussion started: 5 August 2026

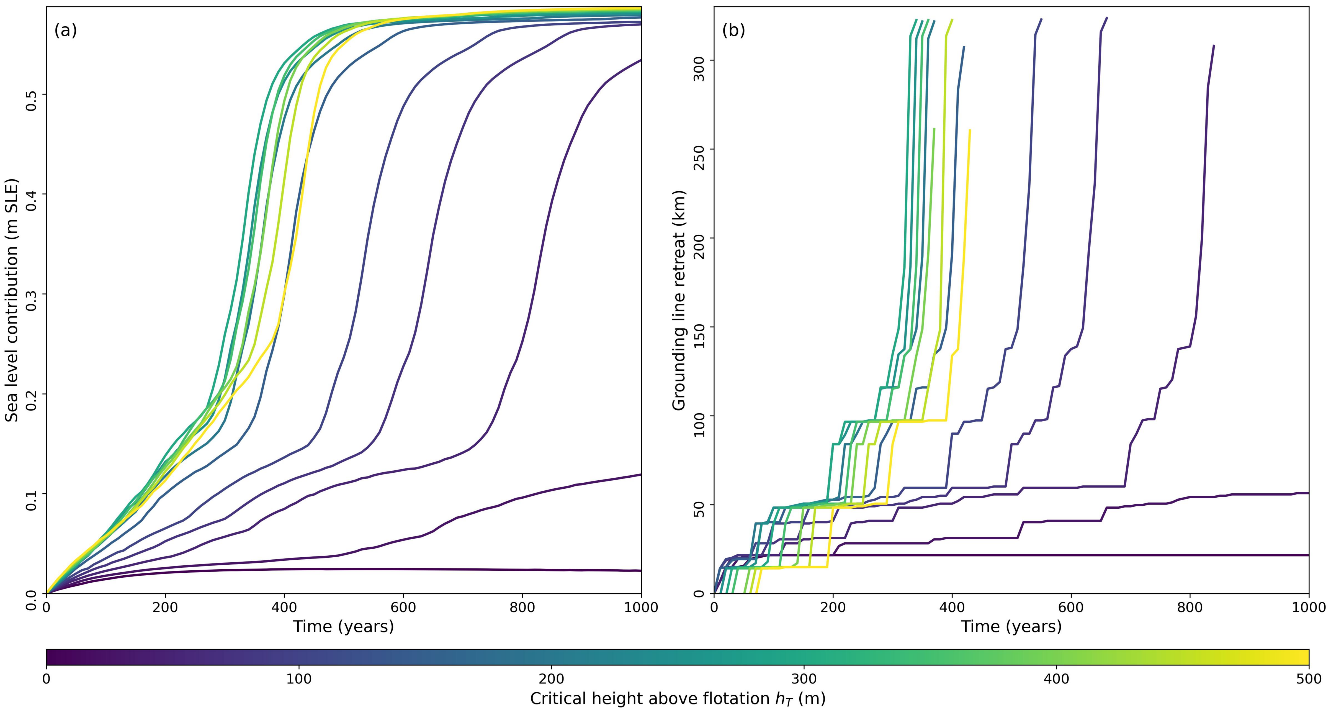

Figure 5. Results for TG1 simulations across the range of h_{T}. (a) and (b) as for Figure 3 but measured within the TG basin.

https://doi.org/10.5194/egusphere-2026-4400
Preprint. Discussion started: 5 August 2026

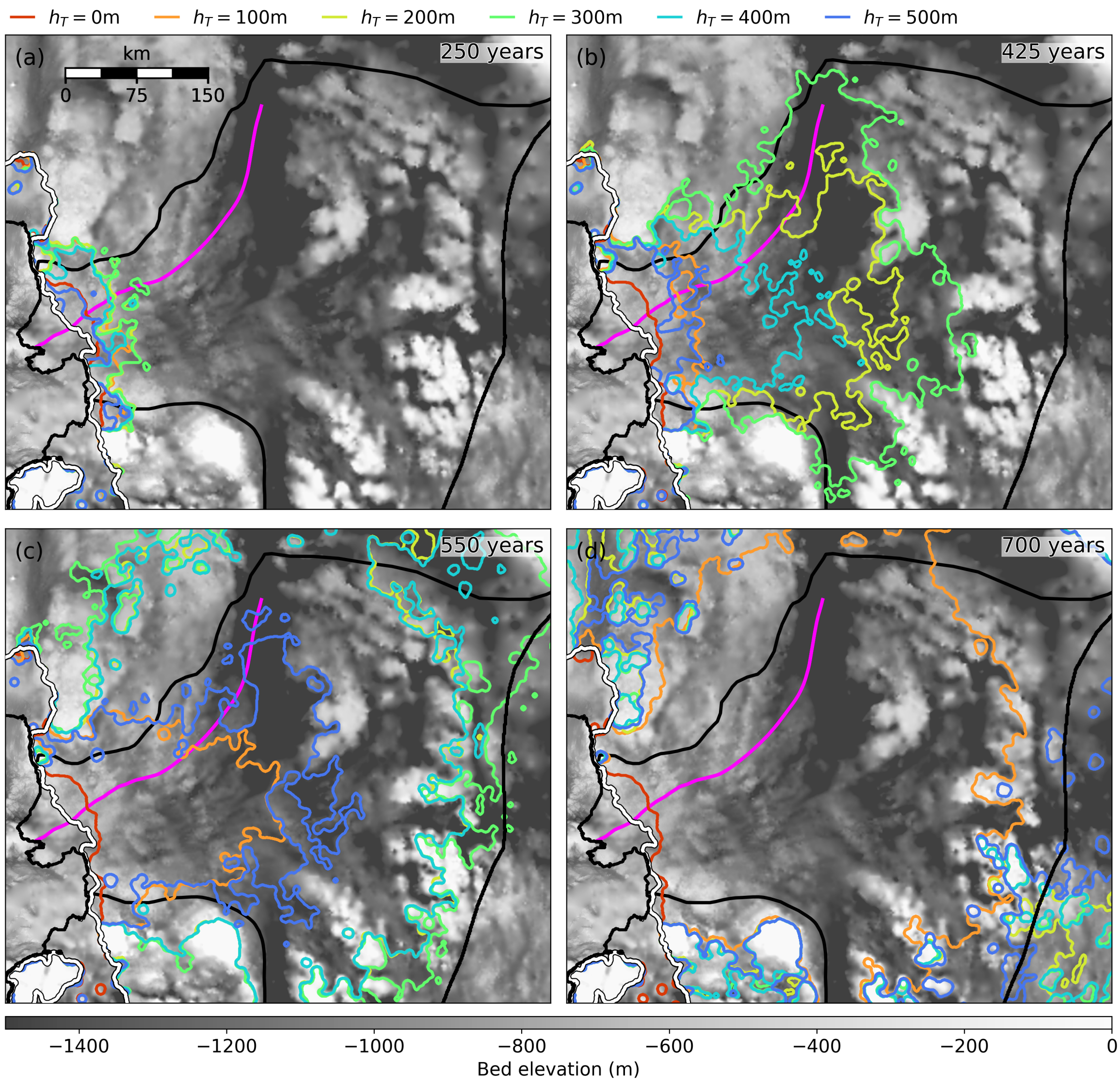

Figure 6. Maps of grounding line retreat for TG1 simulations (Figure 5), across the range of h_{T}. Snapshots at 250 years (a), 425 years (b), 550 years (c) and 700 years (d).

https://doi.org/10.5194/egusphere-2026-4400
Preprint. Discussion started: 5 August 2026

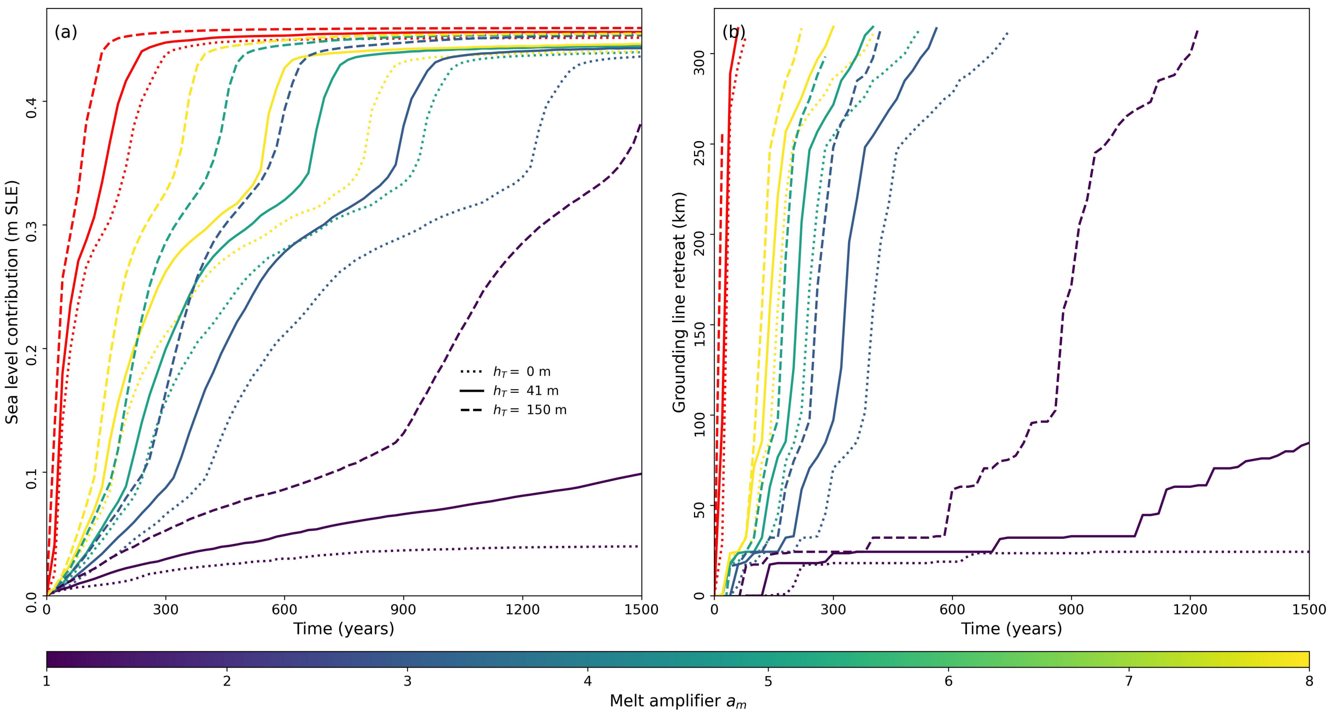

Figure 7. Results for PIG2 simulations for a range of values of the melt amplifier a_{m}, and for three different values of h_{T}. (a) The change in SLC within the PIG basin. (b) The grounding line retreat measured along the PIG flowline. The red lines denote extreme melt simulations in which ice shelves were immediately removed and prohibited from regrowing.

https://doi.org/10.5194/egusphere-2026-4400
Preprint. Discussion started: 5 August 2026

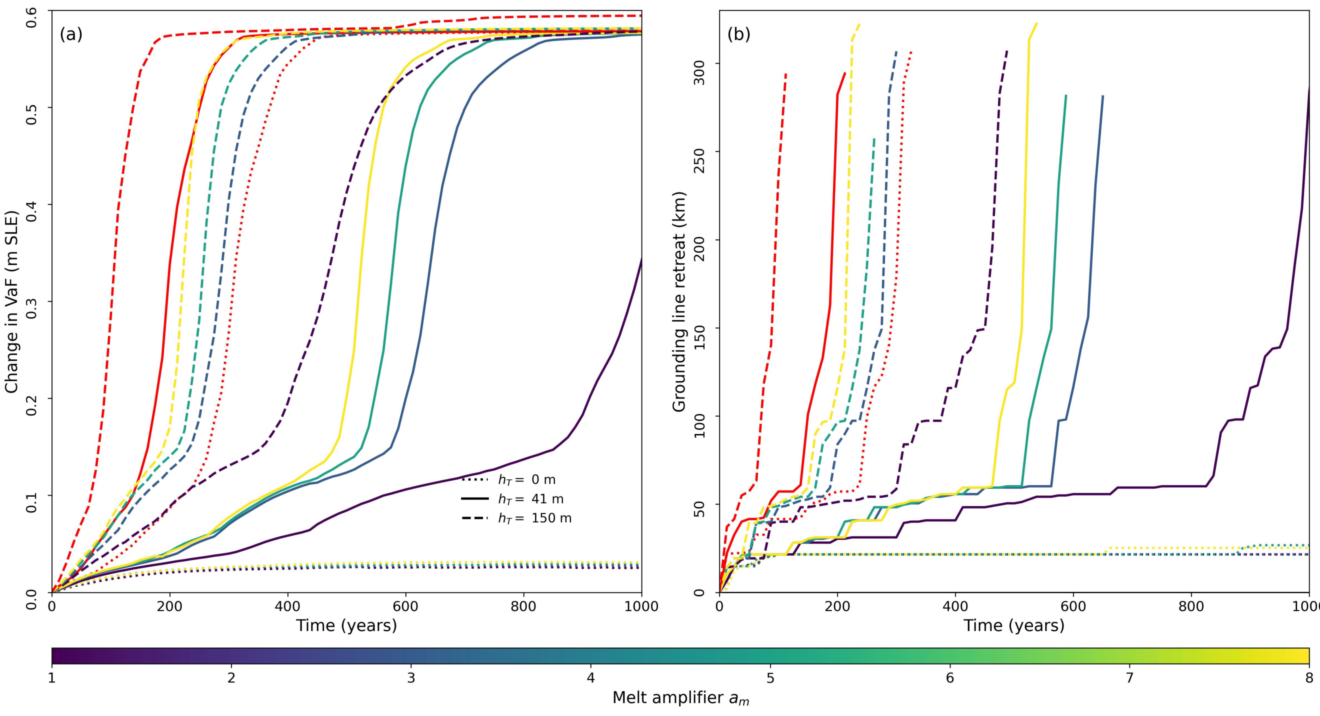

Figure 8. Results for TG2 simulations for a range of values of the melt amplifier a_{m}, and for three different values of h_{T}. (a) and (b) as for Figure 7 but measured within the TG basin.

Code and data availability. The version of the open-source BISICLES ice flow model used in this study is available for download from https://doi.org/10.5281/zenodo.18773165 (Cornford et al., 2026). The MEaSUREs BedMachine Antarctica ice sheet topography (NSIDC-0756, Version 3; https://doi.org/10.5067/FPSU0V1MWUB6, Morlighem (2022)) and the MEaSUREs Phase-Based Antarctica Ice Velocity Map (NSIDC-0754, Version 1; https://doi.org/10.5067/PZ3NJ5RXRH10, Mouginot et al. (2019)) are available from the National Snow and Ice Data Center (NSIDC). The mean 1980 to 2018 Antarctica accumulation rate and surface air temperature from Modèle Atmosphérique Régional (MAR) regional climate model are available at https://doi.org/10.5281/zenodo.2547638 (Agosta and Fettweis, 2019). The mean geothermal heat flux for Antarctica is available from Burton-Johnson et al. (2020). The Antarctic thickness change rate is available at http://hdl.handle.net/1773/45388 (Smith et al., 2020). The scripts and data required to perform these simulations and the output data are available at https://doi.org/10.5281/zenodo.21794928.

Author contributions. MT devised this study, carried out all experiments and analysis and prepared the manuscript with contributions from AJP and SLC.

Competing interests. The authors declare that they have no conflict of interest.

Acknowledgements. Funding for this study was provided by the Natural Environment Reseach Council through the ISOTIPIC project (UKRI-NERC: Grant NE/Z503344/1).

https://doi.org/10.5194/egusphere-2026-4400
Preprint. Discussion started: 5 August 2026

References

Agosta, C. and Fettweis, X.: Antarctic surface mass balance with the regional climate model MAR (1979–2015), https://doi.org/10.5281/zenodo.2547638, 2019.

Agosta, C., Amory, C., Kittel, C., Orsi, A., Favier, V., Gallée, H., van den Broeke, M. R., Lenaerts, J. T. M., van Wessem, J. M., van de Berg, W. J., and Fettweis, X.: Estimation of the Antarctic surface mass balance using the regional climate model MAR (1979–2015) and identification of dominant processes, The Cryosphere, 13, 281–296, https://doi.org/10.5194/tc-13-281-2019, 2019.

Alevropoulos-Borrill, A. V., Nias, I. J., Payne, A. J., Golledge, N. R., and Bingham, R. J.: Ocean-forced evolution of the Amundsen Sea catchment, West Antarctica, by 2100, Cryosphere, 14, 1245–1258, https://doi.org/10.5194/tc-14-1245-2020, 2020.

Barnes, J. M. and Gudmundsson, G. H.: The predictive power of ice sheet models and the regional sensitivity of ice loss to basal sliding parameterisations: a case study of Pine Island and Thwaites glaciers, West Antarctica, Cryosphere, 16, 4291–4304, https://doi.org/10.5194/tc-16-4291-2022, 2022.

Benn, D. I., Luckman, A., Åström, J. A., Crawford, A. J., Cornford, S. L., Bevan, S. L., Zwinger, T., Gladstone, R., Alley, K. E., Pettit, E., and Bassis, J.: Rapid fragmentation of Thwaites Eastern Ice Shelf, Cryosphere, 16, 2545–2564, https://doi.org/10.5194/tc-16-2545-2022, 2022.

Bevan, S., Cornford, S. L., Gilbert, L., Otosaka, I., Martin, D. F., and Surawy-Stepney, T.: Amundsen Sea Embayment ice-sheet mass-loss predictions to 2050 calibrated using observations of velocity and elevation change, Journal of Glaciology, pp. 1–11, https://doi.org/10.1017/jog.2023.57, 2023.

Brondex, J., Gagliardini, O., Gillet-Chaulet, F., and Durand, G.: Sensitivity of grounding line dynamics to the choice of the friction law, Journal of Glaciology, 63, 854–866, https://doi.org/10.1017/jog.2017.51, 2017.

Budd, W. F., Keage, P. L., and Blundy, N. A.: Empirical Studies of Ice Sliding, Journal of Glaciology, 23, 157–170, https://doi.org/10.3189/S0022143000029804, 1979.

Burton-Johnson, A., Dziadek, R., and Martin, C.: Review article: Geothermal heat flow in Antarctica: current and future directions, The Cryosphere, 14, 3843–3873, https://doi.org/10.5194/tc-14-3843-2020, 2020.

Cornford, S., Kachuck, S., Trevers, M., and Mitcham, T.: matttrevers/bisicles-camip: bisicles_mjt_2026, https://doi.org/10.5281/zenodo.18773165, 2026.

Cornford, S. L., Martin, D. F., Graves, D. T., Ranken, D. F., Le Brocq, A. M., Gladstone, R. M., Payne, A. J., Ng, E. G., and Lipscomb, W. H.: Adaptive mesh, finite volume modeling of marine ice sheets, Journal of Computational Physics, 232, 529–549, 2013.

Cornford, S. L., Martin, D. F., Payne, A. J., Ng, E. G., Le Brocq, A. M., Gladstone, R. M., Edwards, T. L., Shannon, S. R., Agosta, C., Van Den Broeke, M. R., Hellmer, H. H., Krinner, G., Ligtenberg, S. R. M., Timmermann, R., and Vaughan, D. G.: Century-scale simulations of the response of the West Antarctic Ice Sheet to a warming climate, Cryosphere, 9, 1579–1600, https://doi.org/10.5194/tc-9-1579-2015, 2015.

Dutrieux, P., Vaughan, D. G., Corr, H. F. J., Jenkins, a., Holland, P. R., Joughin, I., and Fleming, a. H.: Pine Island glacier ice shelf melt distributed at kilometre scales, Cryosphere, 7, 1543–1555, https://doi.org/10.5194/tc-7-1543-2013, 2013.

Favier, L., Durand, G., Cornford, S. L., Gudmundsson, G. H., Gagliardini, O., Gillet-Chaulet, F., Zwinger, T., Payne, A. J., and Le Brocq, A. M.: Retreat of Pine Island Glacier controlled by marine ice-sheet instability, Nature Climate Change, 4, 117–121, https://doi.org/10.1038/nclimate2094, 2014.

https://doi.org/10.5194/egusphere-2026-4400
Preprint. Discussion started: 5 August 2026

Gagliardini, O., Cohen, D., Råback, P., and Zwinger, T.: Finite-element modeling of subglacial cavities and related friction law, Journal of Geophysical Research, 112, F02 027, https://doi.org/10.1029/2006JF000576, 2007.

Gudmundsson, G. H., Barnes, J. M., Goldberg, D. N., and Morlighem, M.: Limited Impact of Thwaites Ice Shelf on Future Ice Loss From Antarctica, Geophysical Research Letters, 50, 1–11, https://doi.org/10.1029/2023gl102880, 2023.

Holland, P. R., Bracegirdle, T. J., Dutrieux, P., Jenkins, A., and Steig, E. J.: West Antarctic ice loss influenced by internal climate variability and anthropogenic forcing, Nature Geoscience, 12, 718–724, https://doi.org/10.1038/s41561-019-0420-9, 2019.

Jenkins, A., Dutrieux, P., Jacobs, S., Steig, E., Gudmundsson, H., Smith, J., and Heywood, K.: Decadal Ocean Forcing and Antarctic Ice Sheet Response: Lessons from the Amundsen Sea, Oceanography, 29, 106–117, https://doi.org/10.5670/oceanog.2016.103, 2016.

Joughin, I., Smith, B. E., Howat, I. M., Scambos, T. A., and Moon, T.: Greenland flow variability from ice-sheet-wide velocity mapping, Journal of Glaciology, 56, 415–430, https://doi.org/10.3189/002214310792447734, 2010a.

Joughin, I., Smith, B. E., and Medley, B.: Marine Ice Sheet Collapse Potentially Under Way for the Thwaites Glacier Basin, West Antarctica, Science, 344, 735–738, https://doi.org/10.1126/science.1249055, 2014.

Joughin, I., Shean, D. E., Smith, B. E., and Floricioiu, D.: A Decade of Variability on Jakobshavn Isbrae: Ocean Temperatures Pace Speed Through Influence on Mélange Rigidity, The Cryosphere Discussions, pp. 1–27, https://doi.org/10.5194/tc-2019-197, 2019.

Joughin, I., Shapero, D., and Dutrieux, P.: Responses of the Pine Island and Thwaites glaciers to melt and sliding parameterizations, The Cryosphere, 18, 2583–2601, https://doi.org/10.5194/tc-18-2583-2024, 2024.

Joughin, I. R., Smith, B. E., and Holland, D. M.: Sensitivity of 21st century sea level to ocean-induced thinning of Pine Island Glacier, Antarctica, Geophysical Research Letters, 37, L20 502,, https://doi.org/10.1029/2010GL044819, 2010b.

Kazmierczak, E., Sun, S., Coulon, V., and Pattyn, F.: Subglacial hydrology modulates basal sliding response of the Antarctic ice sheet to climate forcing, The Cryosphere, 16, 4537–4552, https://doi.org/10.5194/tc-16-4537-2022, 2022.

Lliboutry, L.: General theory of subglacial cavitation and sliding of temperate glaciers, Journal of Glaciology, 7, 21–58, 1968.

Lu, G. and Kingslake, J.: Two-way coupling between ice flow and channelized subglacial drainage enhances modeled marine-ice-sheet retreat, The Cryosphere, 18, 5301–5321, https://doi.org/10.5194/tc-18-5301-2024, 2024.

MacAyeal, D. R.: A tutorial on the use of control methods in ice-sheet modeling, Journal of Glaciology, pp. 91–98, 1993.

Martin, D. F., Cornford, S. L., and Payne, A. J.: Millennial-Scale Vulnerability of the Antarctic Ice Sheet to Regional Ice Shelf Collapse, Geophysical Research Letters, 46, 1467–1475, https://doi.org/10.1029/2018GL081229, 2019.

Miles, B. W. J., Stokes, C. R., Jenkins, A., Jordan, J. R., Jamieson, S. S. R., and Gudmundsson, G. H.: Intermittent structural weakening and acceleration of the Thwaites Glacier Tongue between 2000 and 2018, Journal of Glaciology, 66, 485–495, https://doi.org/10.1017/jog.2020.20, 2020.

Minchew, B. and Joughin, I.: Toward a universal glacier slip law, Science, 368, 29–30, https://doi.org/10.1126/science.abb3566, 2020.

Morlighem, M.: MEaSUREs BedMachine Antarctica, Version 3 [Data Set], https://doi.org/10.5067/FPSU0V1MWUB6, 2022.

Morlighem, M., Rignot, E., Binder, T., Blankenship, D., Drews, R., Eagles, G., Eisen, O., Ferraccioli, F., Forsberg, R., Fretwell, P., Goel, V., Greenbaum, J. S., Gudmundsson, G. H., Guo, J., Helm, V., Hofstede, C., Howat, I., Humbert, A., Jokat, W., Karlsson, N. B., Lee, W. S., Matsuoka, K., Millan, R., Mouginot, J., Paden, J., Pattyn, F., Roberts, J., Rosier, S., Ruppel, A., Seroussi, H., Smith, E. C., Steinhage, D., Sun, B., van den Broeke, M. R., van Ommen, T. D., van Wessem, M., and Young, D. A.: Deep glacial troughs and stabilizing ridges unveiled beneath the margins of the Antarctic ice sheet, Nature Geoscience, 13, 132–137, https://doi.org/10.1038/s41561-019-0510-8, 2020.

https://doi.org/10.5194/egusphere-2026-4400
Preprint. Discussion started: 5 August 2026

Mouginot, J., Rignot, E., and Scheuchl, B.: MEaSUREs Phase-Based Antarctica Ice Velocity Map, Version 1 [Data Set], https://doi.org/https://doi.org/10.5067/PZ3NJ5RXRH10, 2019.

Naughten, K. A., Holland, P. R., Dutrieux, P., Kimura, S., Bett, D. T., and Jenkins, A.: Simulated Twentieth-Century Ocean Warming in the Amundsen Sea, West Antarctica, Geophysical Research Letters, 49, https://doi.org/10.1029/2021GL094566, 2022.

Nias, I. J., Cornford, S. L., and Payne, A. J.: Contrasting the modelled sensitivity of the Amundsen Sea Embayment ice streams, Journal of Glaciology, 62, 552–562, https://doi.org/10.1017/jog.2016.40, 2016.

Nias, I. J., Cornford, S. L., and Payne, A. J.: New Mass-Conserving Bedrock Topography for Pine Island Glacier Impacts Simulated Decadal Rates of Mass Loss, Geophysical Research Letters, 45, 3173–3181, https://doi.org/10.1002/2017GL076493, 2018.

O'Neill, J. F., Edwards, T. L., Martin, D. F., Shafer, C., Cornford, S. L., Seroussi, H. L., Nowicki, S., Adhikari, M., and Gregoire, L. J.: ISMIP6-based Antarctic projections to 2100: simulations with the BISICLES ice sheet model, The Cryosphere, 19, 541–563, https://doi.org/10.5194/tc-19-541-2025, 2025.

Parizek, B. R., Christianson, K., Anandakrishnan, S., Alley, R. B., Walker, R. T., Edwards, R. A., Wolfe, D. S., Bertini, G. T., Rinehart, S. K., Bindschadler, R. A., and Nowicki, S. M. J.: Dynamic (in)stability of Thwaites Glacier, West Antarctica, Journal of Geophysical Research: Earth Surface, 118, 638–655, https://doi.org/10.1002/jgrf.20044, 2013.

Rignot, E., Jacobs, S., Mouginot, J., and Scheuchl, B.: Ice-Shelf Melting Around Antarctica, Science, 341, 266–270, https://doi.org/10.1126/science.1235798, 2013.

Rignot, E., Mouginot, J., Scheuchl, B., van den Broeke, M., van Wessem, M. J., and Morlighem, M.: Four decades of Antarctic Ice Sheet mass balance from 1979–2017, Proceedings of the National Academy of Sciences, 116, 1095–1103, https://doi.org/10.1073/pnas.1812883116, 2019.

Rignot, E., Ciracì, E., Scheuchl, B., Tolpekin, V., Wollersheim, M., and Dow, C.: Widespread seawater intrusions beneath the grounded ice of Thwaites Glacier, West Antarctica, Proceedings of the National Academy of Sciences, 121, e2404766 121, https://doi.org/10.1073/pnas.2404766121, 2024.

Schoof, C.: The effect of cavitation on glacier sliding, Proceedings of the Royal Society A: Mathematical, Physical and Engineering Sciences, 461, 609–627, https://doi.org/10.1098/rspa.2004.1350, 2005.

Schoof, C.: Ice sheet grounding line dynamics: Steady states, stability, and hysteresis, Journal of Geophysical Research, 112, F03S28, 2007.

Schoof, C. and Hindmarsh, R. C. A.: Thin-film flows with wall slip: An asymptotic analysis of higher order glacier flow models, Quarterly Journal of Mechanics and Applied Mathematics, 63, 73–114, https://doi.org/10.1093/qjmam/hbp025, 2010.

Seroussi, H., Nakayama, Y., Larour, E., Menemenlis, D., Morlighem, M., Rignot, E., and Khazendar, A.: Continued retreat of Thwaites Glacier, West Antarctica, controlled by bed topography and ocean circulation, Geophysical Research Letters, 44, 6191–6199, https://doi.org/10.1002/2017GL072910, 2017.

Smith, B. E., Fricker, H. A., Gardner, A. S., Medley, B., Nilsson, J., Paolo, F. S., Holschuh, N., Adusumilli, S., Brunt, K., Csatho, B., Harbeck, K., Markus, T., Neumann, T., Siegfried, M. R., and Zwally, H. J.: Pervasive ice sheet mass loss reflects competing ocean and atmosphere processes, Science, 368, 1239–1242, https://doi.org/10.1126/science.aaz5845, 2020.

Tsai, V. C., Stewart, A. L., and Thompson, A. F.: Marine ice-sheet profiles and stability under Coulomb basal conditions, Journal of Glaciology, 61, 205–215, https://doi.org/10.3189/2015JoG14J221, 2015.

van den Akker, T., Lipscomb, W. H., Leguy, G. R., Bernales, J., and Berends, C. J.: Present-day mass loss rates are a precursor for West Antarctic Ice Sheet collapse, The Cryosphere, 19, 283–301, https://doi.org/10.5194/tc-19-283-2025, 2025.

Weertman, J.: On the Sliding of Glaciers, Journal of Glaciology, 3, 33–38, https://doi.org/10.3189/S0022143000024709, 1957.

https://doi.org/10.5194/egusphere-2026-4400
Preprint. Discussion started: 5 August 2026

Weertman, J.: Stability of the Junction of an Ice Sheet and an Ice Shelf, Journal of Glaciology, 13, 3–11, https://doi.org/10.1017/S0022143000023327, 1974.

Wild, C. T., Alley, K. E., Muto, A., Truffer, M., Scambos, T. A., and Pettit, E. C.: Weakening of the pinning point buttressing Thwaites Glacier, West Antarctica, The Cryosphere, 16, 397–417, https://doi.org/10.5194/tc-16-397-2022, 2022.

Yu, H., Rignot, E., Seroussi, H., and Morlighem, M.: Retreat of Thwaites Glacier, West Antarctica, over the next 100 years using various ice flow models, ice shelf melt scenarios and basal friction laws, The Cryosphere, 12, 3861–3876, https://doi.org/10.5194/tc-12-3861-2018, 2018.

Zoet, L. K. and Iverson, N. R.: A slip law for glaciers on deformable beds, Science, 368, 76–78, https://doi.org/10.1126/science.aaz1183, 2020.

Zwally, H. J., Giovinetoo, M. B., Beckley, M. A., and Saba, J. L.: Antarctic and Greenland Drainage Systems, https://earth.gsfc.nasa.gov/cryo/data/polar-altimetry/antarctic-and-greenland-drainage-systems, 2012.